Journal of Solid State Chemistry 181 (2008) 2783–2788

Contents lists available at ScienceDirect

Journal of Solid State Chemistry

journal homepage: www.elsevier.com/locate/jssc

Synthesis, crystal structures and luminescence properties of the Eu^{3+}-doped yttrium oxotellurates(IV) $Y_2Te_4O_{11}$ and $Y_2Te_5O_{13}$

Patrick Höss [a], Andres Osvet [b], Frank Meister [b], Miroslaw Batentschuk [b], Albrecht Winnacker [b], Thomas Schleid [a,*]

[a] Institute for Inorganic Chemistry, University of Stuttgart, Stuttgart, Germany
[b] Department of Materials Science and Engineering, University of Erlangen, Erlangen, Germany

ARTICLE INFO

Article history:
Received 27 March 2008
Received in revised form
26 June 2008
Accepted 4 July 2008
Available online 11 July 2008

Keywords:
Rare-earth metal(III) compounds
Oxotellurates(IV)
Crystal structures
Photoluminescence spectroscopy

ABSTRACT

$Y_2Te_4O_{11}:Eu^{3+}$ and $Y_2Te_5O_{13}:Eu^{3+}$ single crystals in sub-millimeter scale were synthesized from the binary oxides (Y_2O_3, Eu_2O_3 and TeO_2) using CsCl as fluxing agent. Crystallographic structures of the undoped yttrium oxotellurates(IV) $Y_2Te_4O_{11}$ and $Y_2Te_5O_{13}$ have been determined and refined from single-crystal X-ray diffraction data. In $Y_2Te_4O_{11}$, a layered structure is present where the reticulated sheets consisting of edge-sharing $[YO_8]^{13-}$ polyhedra are interconnected by the oxotellurate(IV) units, whereas in $Y_2Te_5O_{13}$ only double chains of condensed yttrium–oxygen polyhedra with coordination numbers of 7 and 8 are left, now linked in two crystallographic directions by the oxotellurate(IV) entities. The Eu^{3+} luminescence spectra and the decay time from different energy levels of the doped compounds were investigated and all detected emission levels were identified. Luminescence properties of the Eu^{3+} cations have been interpreted in consideration of the now accessible detailed crystallographic data of the yttrium compounds, providing the possibility to examine the influence of the local symmetry of the oxygen coordination spheres.

1. Introduction

Oxotellurates(IV) of the trivalent rare-earth elements are known for different formula types depending on the M_2O_3:TeO_2 molar ratio and the general formula can thus be described as $M_2O_3(TeO_2)_n$. For $n=4$ this results in the composition $M_2Te_4O_{11}$ (M = Y, La–Nd, Sm–Lu) [1–7], whereas $n=5$ leads to the formula type $M_2Te_5O_{13}$ (M = Sc, Y, Dy–Lu) [2,8–10]. Optical absorption and photoluminescence measurements of pure $Nd_2Te_4O_{11}$, $Pr_2Te_4O_{11}$ and $Eu_2Te_4O_{11}$, as well as Pr^{3+}- and Eu^{3+}-doped $Gd_2Te_4O_{11}$ have already been carried out and analyzed according to the crystal-field effect of the single lanthanoid site (symmetry: 1) [11,12]. Due to the absence of *f*-electrons, the yttrium compounds of these two formula types, $Y_2Te_4O_{11}$ [4] and $Y_2Te_5O_{13}$ [9], were chosen as host lattices for doping with Eu^{3+} cations in order to verify and investigate the luminescence properties of the doped compounds $Y_2Te_4O_{11}:Eu^{3+}$ and $Y_2Te_5O_{13}:Eu^{3+}$. Lanthanoid-doped $Y_2Te_4O_{11}$:Ln^{3+} (Ln = Pr, Eu, Tb) has already been proven to show highly efficient luminescence and thus been considered as promising candidate even for LASER materials [13,14]. The strong absorption combined with the efficient luminescence is desirable for LASER applications. A very weak concentration quenching [14] is eventually connected with the specific structure of $Y_2Te_4O_{11}$, namely a two-dimensional lattice separated by oxoditellurate(IV) entities. However, the published luminescence spectra of $Y_2Te_4O_{11}:Eu^{3+}$, more precisely, the ratio of the intensities of the $^5D_0$–$^7F_2$ and $^5D_0$–$^7F_1$ groups does not correlate with known data about the symmetry-free site for Y^{3+}, and therefore also for Eu^{3+} cations in $Y_2Te_4O_{11}:Eu^{3+}$. The spectra were detected with a low resolution in Ref. [14], however it cannot be a reason for the high intensity of the $^5D_0$–$^7F_1$ transition which is characteristic for a site with inversion symmetry. In $Y_2Te_5O_{13}$, where only chains of rare-earth metal(III)–oxygen polyhedra as a partial structure are left [9], the Eu^{3+} spectra and the possible manifestation of their low site symmetry were not investigated at all up to now. Therefore, detailed structural data of these compounds, which were not reported so far, will be useful for further spectroscopic investigations.

2. Experimental

$Y_2Te_4O_{11}:Eu^{3+}$ and $Y_2Te_5O_{13}:Eu^{3+}$ were both synthesized in evacuated fused silica ampoules at 800 °C for 8 days using cesium chloride (CsCl) as fluxing agent. $Y_2Te_4O_{11}:Eu^{3+}$ could be obtained with the exact molar ratio of 1:4 for Y_2O_3/Eu_2O_3 versus TeO_2,

* Corresponding author. Fax: +49 711 685 64241.
E-mail address: schleid@iac.uni-stuttgart.de (Th. Schleid).

0022-4596/$ - see front matter © 2008 Elsevier Inc. All rights reserved.
doi:10.1016/j.jssc.2008.07.002

whereas for $Y_2Te_5O_{13}$:Eu^{3+} a molar ratio of 1:7 was used in order to prevent the additional formation of the TeO_2-poorer compound and to assure a single-phase product. The single crystals of $Y_2Te_5O_{13}$:Eu^{3+} could be easily picked from the bulk, since they were situated above the recrystallized excess of TeO_2. In both cases the amount of Eu_2O_3 as doping agent was chosen to lead to an occupation of approximately 3% of the Y^{3+} positions by Eu^{3+} cations in the host lattices. After removing the flux by washing the bulk with water, the phase purity of the remaining homogeneous products was determined by X-ray powder diffraction showing no crystalline by-products. The crystal structures were determined by X-ray diffraction of selected undoped single crystals on a Nonius κ-CCD single-crystal diffractometer at room temperature. The results of the structure determinations along with atomic parameters and selected interatomic distances can be taken from Tables 1–5. Further details of the crystal structure investigations are available at the Fachinformationszentrum (FIZ) Karlsruhe, D-76344 Eggenstein-Leopoldshafen, Germany (Fax: +49 7247 808 666; E-mail: crysdata@fiz-karlsruhe.de) on quoting the depository numbers CSD-418854 for $Y_2Te_4O_{11}$ and CSD-418855 for $Y_2Te_5O_{13}$.

The photoluminescence spectra of the Eu^{3+}-doped compounds were measured under the excitation of an Ar-ion laser at 363 nm at room temperature and at 17 K. A closed-cycle cryostat was used to achieve the low temperature. The emission was dispersed by a Jobin-Yvon HRS-2 monochromator with a resolution of 0.2 nm, and detected with a Hamamatsu R-453 multiplier with multi-alkaline cathode. The photoluminescence decay curves were recorded with a digital oscilloscope using 30 ns pulses of an excimer laser operating at 308 nm.

Table 1
Crystallographic data for the yttrium oxotellurates(IV) $Y_2Te_4O_{11}$ and $Y_2Te_5O_{13}$ and their determination

Formula	$Y_2Te_4O_{11}$	$Y_2Te_5O_{13}$
Crystal system, space group	Monoclinic, $C2/c$ (no. 15)	Triclinic, $P\bar{1}$ (no. 2)
Formula units	4	2
Lattice constants		
a (pm)	1238.76(8)	695.16(5)
b (pm)	510.68(3)	862.35(7)
c (pm)	1601.93(9)	1057.49(9)
α (°)	90	89.004(8)
β (°)	106.154(7)	86.843(8)
γ (°)	90	75.038(8)
Calculated density (D_x, g cm^{-3})	5.897	5.560
Molar volume (V_m, cm^3 mol^{-1})	146.57	184.17
$F(0\,0\,0)$	1496	884
Diffractometer, wavelength	κ-CCD (Nonius), Mo$K\alpha$: $\lambda = 71.07$ pm	
Index range		
$\pm h$	16	9
$\pm k$	6	11
$\pm l$	20	13
θ range		
θ_{min}	1.0	1.0
θ_{max}	27.5	27.5
Absorption coefficient (μ, mm^{-1})	23.67	21.20
Data corrections	Background, polarization, and Lorentz factors; numerical absorption correction: program *HABITUS* [15]	
Collected, unique reflections	10042, 1125	19556, 2807
R_{int}, R_σ	0.044, 0.026	0.053, 0.030
Structure solution and refinement	Program package *SHELX–97* [16]	
Scattering factors	International Tables, vol. C [17]	
R_1, reflections with $\lvert F_o\rvert \geq 4\sigma(F_o)$	0.022, 1125	0.024, 2599
R_1, wR_2 for all reflections	0.024, 0.052	0.027, 0.052
Goodness of Fit (GooF)	1.098	1.070
Residual electron density, (ρ, e$^-$ × 10^{-6} pm^{-3})		
max	0.87	0.88
min	−1.53	−1.41

Table 2
Atomic coordinates and equivalent isotropic thermal displacement parameters U_{eq}[a] for the yttrium oxotellurate(IV) $Y_2Te_4O_{11}$

Atom	Wyckoff site	x/a	y/b	z/c	U_{eq} (pm^2)
Y	8*f*	0.11946(3)	0.25253(8)	0.03699(3)	67(1)
Te1	8*f*	0.12771(2)	0.27797(7)	0.37326(2)	72(1)
Te2	8*f*	0.12169(2)	0.72381(7)	0.20018(2)	86(1)
O1	8*f*	0.2508(2)	0.0595(5)	0.3717(2)	133(5)
O2	8*f*	0.2074(2)	0.5428(5)	0.4461(2)	132(5)
O3	8*f*	0.0695(2)	0.1098(5)	0.4545(2)	126(5)
O4	8*f*	0.4747(2)	0.0847(5)	0.4041(2)	116(5)
O5	8*f*	0.3509(2)	0.5570(5)	0.3311(2)	140(5)
O6	4*e*	0	0.8529(7)	1/4	174(8)

[a] $U_{eq} = 1/3[U_{22}+1/\sin^2\beta(U_{11}+U_{22}+2U_{13}\cos\beta)]$ [18].

Table 3
Selected interatomic distances (d, pm) for the yttrium oxotellurate(IV) $Y_2Te_4O_{11}$

Y–O3	225.8	Te1–O3	186.3	Te2–O5	183.2
Y–O5	227.3	Te1–O2	187.7	Te2–O4	190.1
Y–O2	229.8	Te1–O1	189.5	Te2–O6	200.3
Y–O2′	234.5	*Te1–O4*	*261.0*	*Te2–O1*	*235.4*
Y–O1	239.6				
Y–O4	242.3				
Y–O3′	249.2				
Y–O4′	251.3				

Italic terms represent the secondary Te-O-contacts.

Table 4
Atomic coordinates and equivalent isotropic thermal displacement parameters U_{eq}[a] for the yttrium oxotellurate(IV) $Y_2Te_5O_{13}$

Atom	Wyckoff site	x/a	y/b	z/c	U_{eq} (pm^2)
Y1	2*i*	0.44621(7)	0.47349(6)	0.82091(4)	88(1)
Y2	2*i*	0.00193(7)	0.26245(6)	0.76091(4)	92(1)
Te1	2*i*	0.43645(5)	0.90372(4)	0.30201(3)	101(1)
Te2	2*i*	0.12096(5)	0.34748(4)	0.11211(3)	92(1)
Te3	2*i*	0.27676(5)	0.39104(4)	0.48540(3)	97(1)
Te4	2*i*	0.84351(5)	0.19457(4)	0.36324(3)	101(1)
Te5	2*i*	0.70936(5)	0.12031(4)	0.02430(3)	91(1)
O1	2*i*	0.3308(5)	0.2213(4)	0.7783(3)	126(7)
O2	2*i*	0.5369(5)	0.3274(4)	0.0024(3)	128(7)
O3	2*i*	0.2359(5)	0.4929(4)	0.1878(3)	118(7)
O4	2*i*	0.3131(5)	0.7375(4)	0.2875(3)	126(7)
O5	2*i*	0.6619(5)	0.4889(4)	0.3843(3)	143(8)
O6	2*i*	0.0639(5)	0.2638(4)	0.2797(3)	164(8)
O7	2*i*	0.3451(5)	0.9848(4)	0.1249(3)	134(7)
O8	2*i*	0.0485(5)	0.3483(4)	0.5638(3)	158(8)
O9	2*i*	0.4620(5)	0.1921(4)	0.5200(3)	159(8)
O10	2*i*	0.1213(5)	0.4927(4)	0.8909(3)	146(8)
O11	2*i*	0.0604(5)	0.8217(4)	0.0369(3)	141(8)
O12	2*i*	0.6700(5)	0.2573(4)	0.2325(3)	167(8)
O13	2*i*	0.0631(5)	0.0166(4)	0.6865(3)	241(9)

[a] $U_{eq} = 1/3[U_{11}(aa^*)^2+U_{22}(bb^*)^2+U_{33}(cc^*)^2+2U_{12}aba^*b^*\cos\gamma+2U_{13}aca^*c^*\cos\beta+2U_{23}bcb^*c^*\cos\alpha]$ [18].

3. Structure description

$Y_2Te_4O_{11}$ crystallizes monoclinically ($a = 1238.76(8)$ pm, $b = 510.68(3)$ pm, $c = 1601.93(9)$ pm, $\beta = 106.154(7)°$) in the space group $C2/c$ (no. 15) with four formula units per unit cell (Table 1). The structure contains one symmetry-free yttrium site (Wyckoff position: 8*f*) with a coordination sphere of eight oxygen atoms in the shape of a distorted trigonal dodecahedron around the Y^{3+} cations with $d(Y^{3+}–O^{2-}) = 226–251$ pm (Fig. 1). The trigonal dodecahedra share three edges each and build-up

Table 5
Selected interatomic distances (d, pm) for the yttrium oxotellurate(IV) $Y_2Te_5O_{13}$

Y1–O3	229.9	Te1–O4	186.3	Te4–O13	184.3
Y1–O10	230.3	Te1–O1	186.6	Te4–O12	186.5
Y1–O2	230.4	Te1–O7	206.3	Te4–O6	194.7
Y1–O12	232.3	Te1–O9	212.5	*Te4–O5*	*253.4*
Y1–O5	232.6				
Y1–O4	239.0	Te2–O3	186.4	Te5–O11	187.6
Y1–O1	255.9	Te2–O10	188.2	Te5–O2	189.5
Y1–O2′	258.7	Te2–O6	196.1	Te5–O7	193.6
		Te2–O10′	*263.4*	*Te5–O12*	*248.5*
Y2–O13	220.3	*Te2–O11*	*272.9*		
Y2–O8	223.5				
Y2–O1	223.9	Te3–O8	186.7		
Y2–O4	227.6	Te3–O5	186.9		
Y2–O11	230.0	Te3–O9	190.4		
Y2–O3	237.0	*Te3–O8′*	*281.1*		
Y2–O10	275.5				

Italic terms represent the secondary Te-O-contacts.

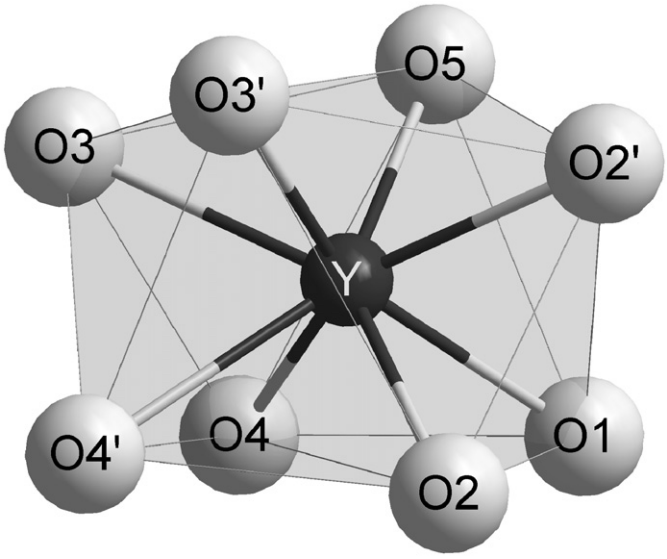

Fig. 1. Coordination polyhedron in the shape of a distorted trigonal dodecahedron about the Y^{3+} cation in the crystal structure of the yttrium oxotellurate(IV) $Y_2Te_4O_{11}$.

reticulated layers according to $[Y_2O_{10}]^{14-}$ parallel to the (0 0 1) plane. The two tellurium sites are coordinated by three oxide anions ($d(Te^{4+}–O^{2-}) = 183–200$ pm) in primary coordination sphere building ψ^1-tetrahedra $[TeO_3]^{2-}$ together with the lone pairs at the Te^{4+} cations. Both oxotellurate(IV) moieties have strong secondary contacts to a fourth oxide anion ($d'(Te^{4+}\cdots O^{2-}) = 235$ and 261 pm, printed in italics in Table 3), however, belonging to the primary coordination sphere of the other Te^{4+} cation resulting in two types of chains of alternating $[(Te1)O_3]^{2-}$ and $[(Te2)O_3]^{2-}$ units, one running successively along [1 1 0] above and the other along [$\bar{1}$ 1 0] below the reticulated layers formed by the $[YO_8]^{13-}$ trigonal dodecahedra. These two chain types are linked together by two Te2 atoms sharing the same O6 atom (Wyckoff position: 4*e*) forming a oxoditellurate(IV) unit $[(Te2)_2O_5]^{2-}$, O6 is furthermore the only oxygen atom not belonging to the coordination sphere of the Y^{3+} cation. Thus, the oxotellurate(IV) partial structure emerges as meshed layers between the reticulated $[Y_2O_{10}]^{14-}$ sheets (Fig. 2) with the meshes accommodating the stereochemically active lone pairs of the Te^{4+} cations. Disregarding the strong secondary $Te^{4+}\cdots O^{2-}$ interactions, the structure of $Y_2Te_4O_{11}$ could also be formulated

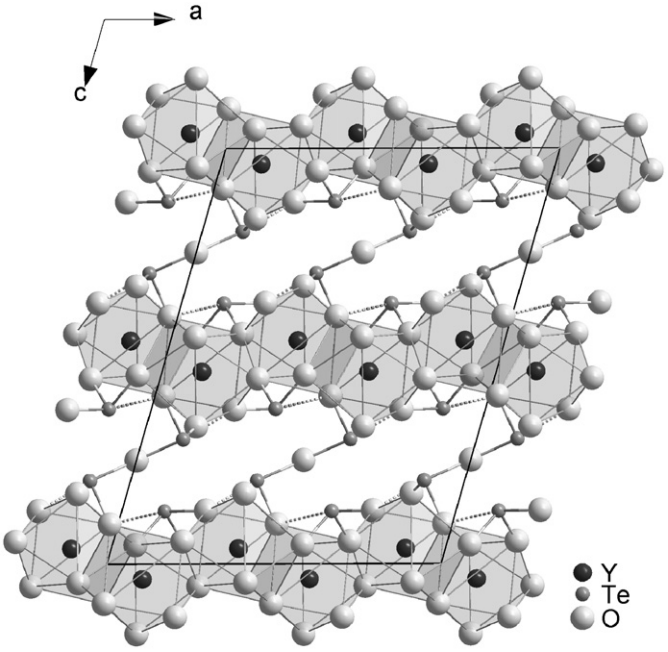

Fig. 2. View at the crystal structure of the yttrium oxotellurate(IV) $Y_2Te_4O_{11}$ along [0 1 0].

according to $Y_2[TeO_3]_2[Te_2O_5]$ with solely the oxoditellurate(IV) unit $[Te_2O_5]^{2-}$ connecting the $[Y_2O_{10}]^{14-}$ layers.

The TeO_2-richer compound $Y_2Te_5O_{13}$ crystallizes in the triclinic system ($a = 695.16(5)$ pm, $b = 862.35(7)$ pm, $c = 1057.49(9)$ pm, $\alpha = 89.004(8)°$, $\beta = 86.843(8)°$, $\gamma = 75.038(8)°$) with the space group $P\bar{1}$ (no. 2) and two formula units per unit cell (Table 1). All atoms occupy symmetry-free sites 2*i* (Table 4). The two crystallographically independent yttrium cations are eight-fold (Y1; $d((Y1)^{3+}–O^{2-}) = 230–259$ pm) and seven-fold (Y2; $d((Y2)^{3+}–O^{2-}) = 220–275$ pm) coordinated by oxygen atoms, respectively (Fig. 3). The resulting coordination polyhedra, a bicapped trigonal prism for $(Y1)^{3+}$ and a distorted pentagonal bipyramid for $(Y2)^{3+}$, build-up chains in direction of the *a*-axis through alternating edge condensation. These chains are further fused to double chains by an additional shared edge between two $[(Y1)O_8]^{13-}$ polyhedra. The oxotellurate(IV) units consist of five tellurium sites, four of them are coordinated by three oxide anions each ($d(Te^{4+}–O^{2-}) = 186–206$ pm), that form together with the lone pairs ψ^1-tetrahedra $[TeO_3]^{2-}$ again, whereas the fifth is surrounded by four oxygen atoms resulting in a ψ^1-trigonal bipyramid $[TeO_4]^{4-}$ ($d((Te1)^{4+}–O^{2-}) = 186–214$ pm). The oxotellurate(IV) units connect the double chains of yttrium–oxygen polyhedra along [0 1 0] through O^{2-}–Te^{4+}–O^{2-}-bridges (Fig. 4, bottom) and along [0 0 1] only by the strong secondary $Te^{4+}\cdots O^{2-}$-contacts ($d(Te^{4+}\cdots O^{2-}) = 249–281$ pm, printed in italics in Table 5) between the $[TeO_3]^{2-}$ entities (Fig. 4, top).

4. Photoluminescence spectroscopy

The low-temperature photoluminescence spectrum of the $Y_2Te_5O_{13}$:Eu^{3+} sample is shown in Fig. 5. The orange emission contains groups of spectral lines characteristic to the Eu^{3+} cations. Most of the lines can be easily identified as transitions between the ^5D_J and ^7F_J terms. The absence of a center of symmetry at yttrium sites occupied by Eu^{3+} allows mixing of the 4*f* orbitals with the orbitals of opposite parity and enables the electric dipole transitions $^5D_0$–$^7F_2$ and $^5D_0$–$^7F_4$. The hypersensitive transition with $\Delta J = 2$ prevails in the spectrum and its integrated intensity

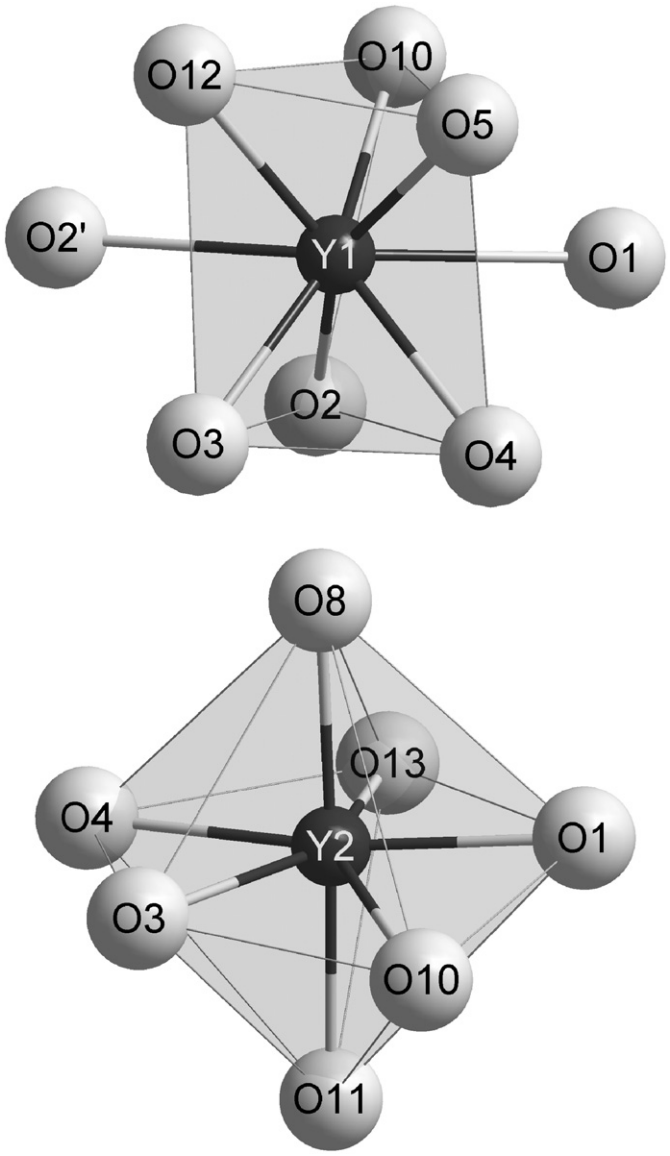

Fig. 3. Coordination polyhedron about the $(Y1)^{3+}$ (top) and the $(Y2)^{3+}$ cations (bottom) in the crystal structure of the yttrium oxotellurate(IV) $Y_2Te_5O_{13}$.

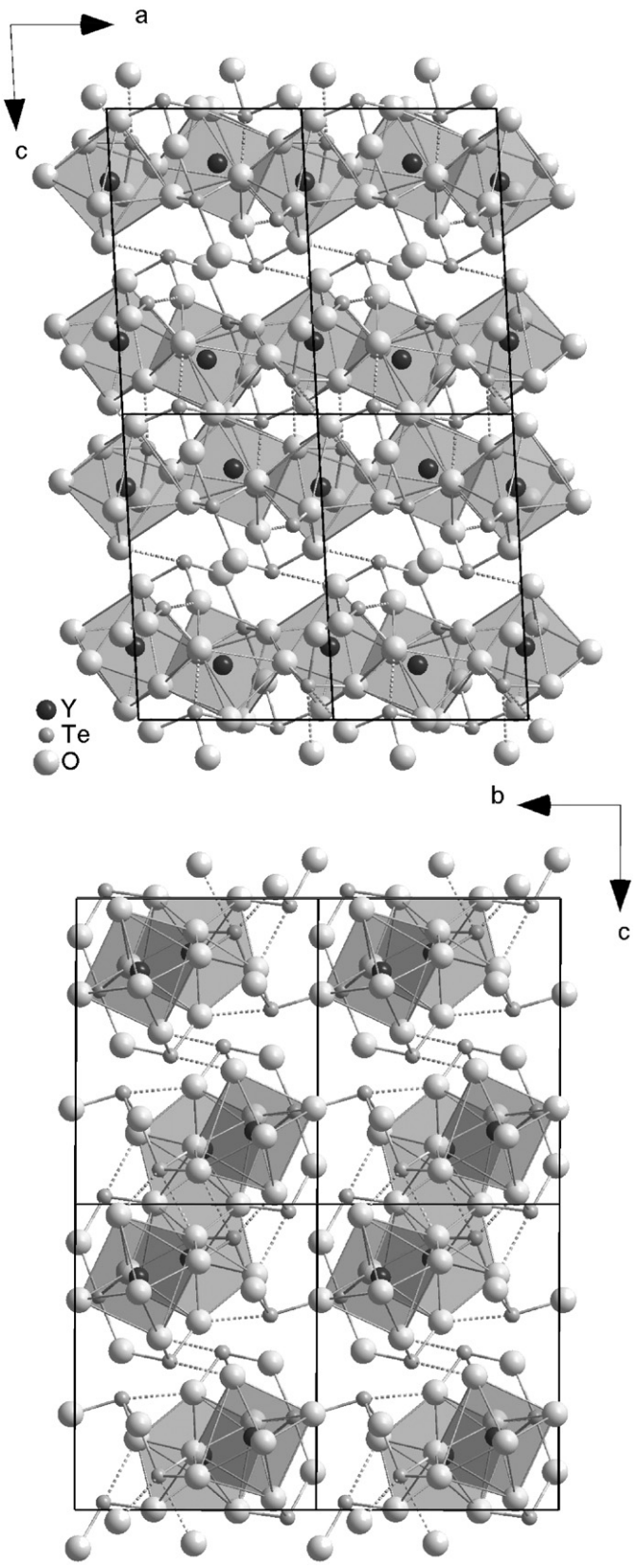

Fig. 4. View at the crystal structure of the yttrium oxotellurate(IV) $Y_2Te_5O_{13}$ along [0 1 0] (top) and [1 0 0] (bottom).

exceeds that of the magnetic dipole transition $^5D_0$–$^7F_1$ by a factor of 2. The $^5D_0$–$^7F_3$ transition, allowed due to mixing between the F_J states, is also recognized in the spectrum. The complete lifting of the degeneracy in crystal field and splitting of the $^5D_0$–$^7F_1$ into three and the $^5D_0$–$^7F_2$ into five components is consistent with the very low symmetry of the Y sites, occupied by Eu^{3+}. The sharp line at 580.4 nm is tentatively interpreted as the $^5D_0$–$^7F_0$ transition. The mechanism of this forbidden transition in the oxotellurates is not known, but a mixing of the states characterized by $J = 0$ and $J = 2$ or 4 may be suggested to account for its existence. Presence of two different sites for Eu^{3+} ions suggests an appearance of two $^5D_0$–$^7F_0$ lines, but unambiguous identification is difficult because a number of lines belonging to the $^5D_1$–$^7F_3$ group can be found in the same spectral region. Splitting of the $^5D_0$–$^7F_1$ into three and $^5D_0$–$^7F_2$ into five components, however, supports the presence of only one emitting site. This may be a result of energy transfer between the sites. Further study by excitation spectroscopy is required to clarify the structure in detail. In the short-wavelength part of the spectrum weak lines belonging to relaxation from the $^5D_1$, $^5D_2$ and $^5D_3$ levels can be recognized. These transitions have a rapid decay (see Fig. 7) and a much higher thermal sensitivity. Nonradiative relaxation to the $^5D_0$ state involving multiple phonons and cross-relaxation between nearby Eu^{3+}

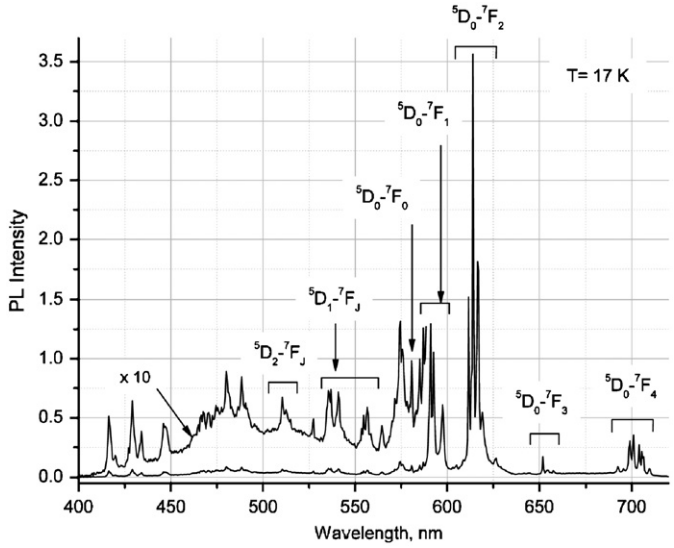

Fig. 5. Photoluminescence spectrum of the $Y_2Te_5O_{13}$:Eu^{3+} sample measured at 17 K and excited by 363 nm Ar-ion laser.

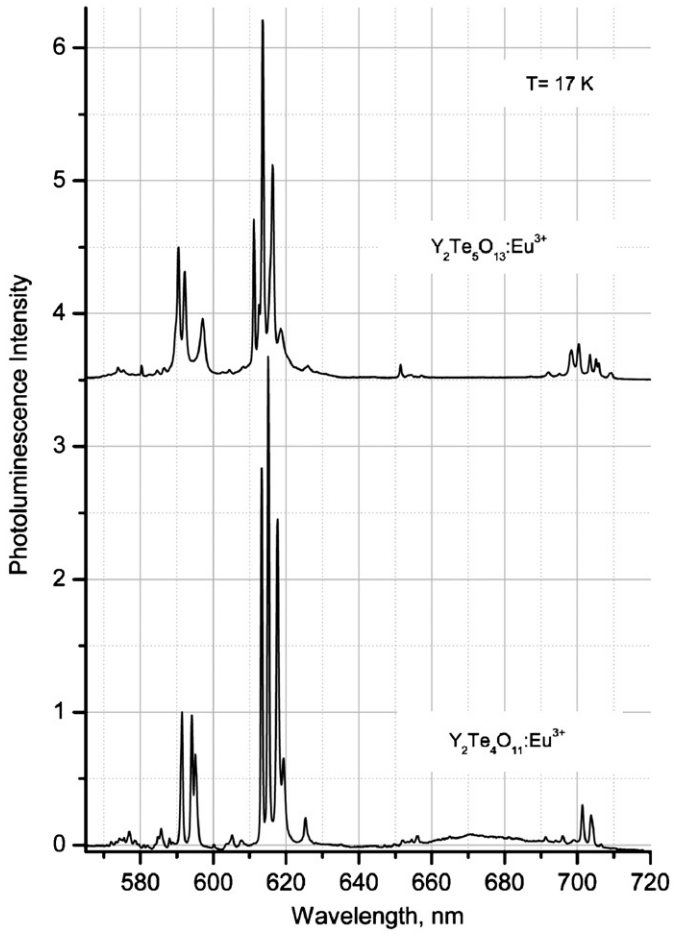

Fig. 6. Photoluminescence spectra of $Y_2Te_5O_{13}$:Eu^{3+} (upper curve) and $Y_2Te_4O_{11}$:Eu^{3+} (lower curve) measured at 17 K (excitation at 363 nm).

cations (note that the sample is doped with 3% Eu^{3+}) is the reason for the weakness of the lines.

The luminescence spectrum of the $Y_2Te_4O_{11}$:Eu^{3+} sample, shown in Fig. 6 (lower curve), is similar to the spectrum of

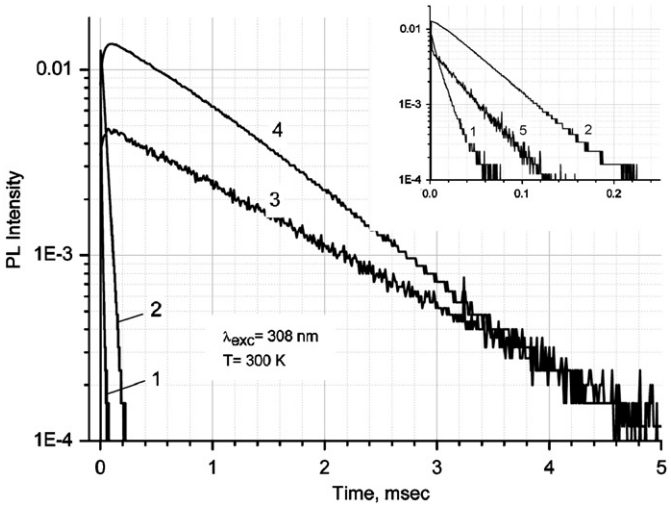

Fig. 7. Photoluminescence decay curves detected at 510 nm (transitions from $^5D_2$, curve 1), 536 nm (transitions from $^5D_1$, curves 2 and 5) and 616 nm (transition $^5D_0$–$^7F_2$, curves 3 and 4). Excitation at 308 nm, $T = 300$ K. Curves 1, 2 and 4 belong to the sample $Y_2Te_4O_{11}$:Eu^{3+}, curves 3 and 5 to the sample $Y_2Te_5O_{13}$:Eu^{3+}.

$Y_2Te_5O_{13}$:Eu^{3+} (shown in the upper curve for comparison). Here the ratio of the intensities of the $^5D_0$–$^7F_2$ and $^5D_0$–$^7F_1$ groups is even higher (2.8) suggesting a stronger mixing of the opposite parity wavefunctions by the crystal field in the $[EuO_8]^{13-}$ polyhedra. This contradicts the results by Endo et al. [14], who conclude that the Y^{3+} site has approximately inverse symmetry. In accordance to our results, Cascales et al. [11] also proved by optical measurements on isotypic $Eu_2Te_4O_{11}$ and $Gd_2Te_4O_{11}$:Eu^{3+} the low site symmetry of the crystallographic unique rare-earth metal cation. At room temperature, the spectral lines are slightly broader (not shown) and the emission has lost approximately 50% of its intensity due to thermal quenching.

Fig. 7 presents the decay curves of photoluminescence detected at different spectral lines. Excitation of the Eu^{3+} cations to their higher energy states by the laser pulse at 308 nm is followed by a rapid relaxation to the $^5D_3$ state. The fairly large separation between the ^5D_J states makes it possible to observe luminescence from all the ^5D_J states. The $^5D_0$ state is populated both by nonradiative relaxation from higher states, or via cross-relaxation between Eu^{3+} cations. This can be seen in Fig. 7 as an intensity build-up in curves 3 and 4. At longer times, the decay of the $^5D_0$ state is exponential with $\tau = 0.9$ ms for the $Y_2Te_4O_{11}$:Eu^{3+} sample and $\tau = 1.3$ ms for the $Y_2Te_5O_{13}$:Eu^{3+} sample. The higher relaxation rate in the former sample is in accordance with its higher $^7F_2/^7F_1$ ratio in the luminescence spectra, which shows that the transition is less forbidden. The decay of the lines at about 536 and 510 nm is more rapid, the lifetime being 46 and 12 μs, respectively, in the $Y_2Te_4O_{11}$:Eu^{3+} sample. This supports the identification of the lines as belonging to transitions from the $^5D_1$ and $^5D_2$ states, respectively. The slight non-exponentiality of the decay curves gives evidence of the energy transfer via cross-relaxation between the ions. As Eu^{3+} occupies the Y^{3+} sites it is reasonable to suggest that cross-relaxation and possibly the migration of excitation energy takes place preferentially in the planes of yttrium–oxygen trigonal dodecahedra, where the minimal possible distances between Eu^{3+} cations are smaller (about 500 pm in $Y_2Te_4O_{11}$ and 390 pm in $Y_2Te_5O_{13}$) than the distance between the planes (1600 pm). Such two-dimensional energy migration has been suggested also by Endo et al. [14] in lanthanoid-cation doped $Y_2Te_4O_{11}$.

5. Conclusions

$Y_2Te_4O_{11}$ and $Y_2Te_5O_{13}$ single crystals in sub-millimeter scale, doped with 3% Eu^{3+}, were synthesized from the binary oxides using CsCl as fluxing agent. The detailed crystallographic data and atomic coordinates as well as equivalent isotropic thermal displacement parameters for the yttrium oxotellurates(IV) $Y_2Te_4O_{11}$ and $Y_2Te_5O_{13}$ were determined. For the latter, it was shown that the oxotellurate(IV) units connect the double chains of yttrium–oxygen polyhedra along [0 1 0] through O^{2-}–Te^{4+}–O^{2-}-bridges and along [0 0 1] only by the strong secondary $Te^{4+}\cdots O^{2-}$-contacts ($d(Te^{4+}\cdots O^{2-}) = 249$–$281$ pm) between the $[TeO_3]^{2-}$ entities. $Y_2Te_5O_{13}$ is therefore an excellent example showing the importance of the strong secondary $Te^{4+}\cdots O^{2-}$ interactions for the crystal structures of the rare-earth metal(III) oxotellurates(IV).

The Eu^{3+} luminescence spectra and the decay time from different energy levels were investigated. Although two differently (seven- and eight-fold) coordinated sites are possible for the Eu^{3+} ions in $Y_2Te_5O_{13}$, the observation of only one $^5D_0$–$^7F_0$ line and the character of splitting of $^5D_0$–^7F_J manifolds shows that only one site is active in the photoluminescence. A stronger mixing of the opposite parity states by crystal field in the $[EuO_8]^{13-}$ polyhedra in $Y_2Te_4O_{11}$ than in $Y_2Te_5O_{13}$ was concluded from the ratio of the luminescence intensities of the $^5D_0$–$^7F_2$ and $^5D_0$–$^7F_1$ manifolds.

Acknowledgments

We thank Dr. Ingo Hartenbach for the measurement of the X-ray single-crystal diffraction data sets. Furthermore we gratefully acknowledge the "Land Baden-Württemberg" (Stuttgart), the "Fonds der Chemischen Industrie" (Frankfurt a. M.), and the "Deutsche Forschungsgemeinschaft" (DFG, Bonn) within the *Schwerpunktprogramm 1166*: "Lanthanoidspezifische Funktionalitäten in Molekül und Material" for considerable financial support.

References

[1] A. Castro, R. Enjalabert, D. Lloyd, I. Rassines, J. Galy, J. Solid State Chem. 85 (1990) 100–107.
[2] F.A. Weber, S.F. Meier, Th. Schleid, Z. Anorg. Allg. Chem. 627 (2001) 2225–2231.
[3] S.F. Meier, Th. Schleid, Z. Naturforsch. 59b (2004) 881–889.
[4] P. Höss, S.F. Meier, Th. Schleid, Z. Kristallogr. Suppl. 21 (2004) 162.
[5] I. Ijjali, C. Flaschenriem, J.A. Ibers, J. Alloys Compd. 354 (2003) 115–119.
[6] Y.-L. Shen, J.-G. Mao, J. Alloys Compd. 385 (2004) 86–89.
[7] P. Höss, G. Starkulla, Th. Schleid, Acta Crystallogr. E 61 (2005) i113–i115.
[8] S.F. Meier, Th. Schleid, Z. Naturforsch. 60b (2005) 720–726.
[9] P. Höss, S.F. Meier, Th. Schleid, Z. Kristallogr. Suppl. 22 (2005) 153.
[10] P. Höss, Th. Schleid, Z. Anorg. Allg. Chem. 633 (2007) 1391–1396.
[11] C. Cascales, E. Antic-Fidancev, M. Lemaitre-Blaise, P. Porcher, J. Alloys Compd. 180 (1992) 111–116.
[12] C. Cascales, E. Antic-Fidancev, M. Lemaitre-Blaise, P. Porcher, J. Phys.: Condens. Matter 4 (1992) 2721–2734.
[13] T. Endo, A. Shibuya, T. Sato, M. Shimada, J. Solid State Chem. 78 (1989) 237–241.
[14] T. Endo, A. Shibuya, H. Takizawa, M. Shimada, J. Alloys Compd. 192 (1993) 50–52.
[15] W. Herrendorf, H. Bärnighausen, HABITUS: program for the optimization of the crystal shape for numerical absorption correction in XSHAPE (version 1.06, Fa. Stoe, Darmstadt 1999), Karlsruhe, Gießen, Germany, 1993, 1996.
[16] G.M. Sheldrick, SHELX97: program package for solution and refinement of crystal structures from X-ray diffraction data, Göttingen, Germany, 1997.
[17] Th. Hahn, A.J.C. Wilson (Eds.), International Tables for Crystallography, vol. C, Kluwer Academic Publishers, Boston, Dordrecht, London, 1992.
[18] R.X. Fischer, E. Tillmanns, Acta Crystallogr. C 44 (1988) 775–776.